ACS Catalysis

Research Article

pubs.acs.org/acscatalysis

# Highly Efficient $CdS/WO_3$ Photocatalysts: Z-Scheme Photocatalytic Mechanism for Their Enhanced Photocatalytic $H_2$ Evolution under Visible Light

Li J. Zhang,[†] Shuo Li,[†] Bing K. Liu,[†] De J. Wang,[†,‡] and Teng F. Xie*[,†]

[†]State Key Laboratory of Theoretical and Computational Chemistry, College of Chemistry, Jilin University, Changchun, Jilin 130012, People's Republic of China

[‡]Department of Chemistry, Tsinghua University, Beijing 100084, People's Republic of China

Supporting Information

**ABSTRACT:** Natural photosynthesis is usually recognized as an efficient mechanism to achieve solar energy conversion. We construct a $CdS/WO_3$ nanojunction achieving a Z-scheme for clean hydrogen fuel evolution by mimicking the natural photosynthesis. Although $WO_3$ alone cannot be used for $H_2$ evolution from water splitting, it can significantly increase the $H_2$ evolution activity of CdS through a Z-scheme mechanism with lactate as electron donor. The $CdS/WO_3$ photocatalyst has a high $H_2$ evolution rate of 369 $\mu$mol $g^{-1}$ $h^{-1}$ at a CdS concentration of 20 wt %, which is 5 times as high as that of CdS with lactic acid as electron donor. For further improving the hydrogen production rate, we introduce the noble metal Pt to ameliorate the charge transport between CdS and $WO_3$. Good $H_2$ evolution rates up to 2900 $\mu$mol $g^{-1}$ $h^{-1}$ were obtained with WPC3, which is about 7.9 times the rate of WC20 with visible radiation. The interesting thing is that the photocatalytic mechanism of $CdS/WO_3$ is different from the previously reported mechanism. The results of TPV (transient photovoltage) and SPV (surface photovoltage) indicate that the Z-scheme system of $CdS/WO_3$ can effectively promote charge separation and depress the charges recombining of photogenerated charge in CdS, based on the Z-scheme mechanism, resulting in efficient $H_2$ production activity under visible light.

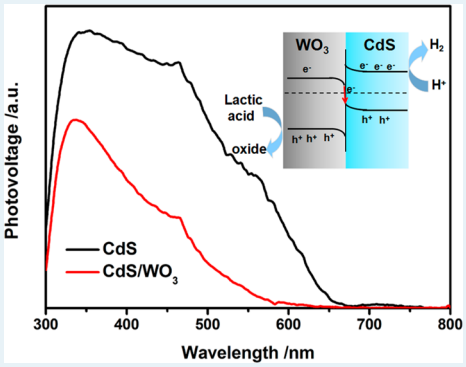


**KEYWORDS:** *CdS, photocatalytic $H_2$ evolution, Z-scheme, surface photovoltage, photogenerated charge transfer, $WO_3$*

## INTRODUCTION

Photoinduced water decomposing into $H_2$ using photocatalyzers is considered as a leading edge study field as a result of increasing attention to environment as well as excessive consumption of fossil power.[1−7] Compared to single-phase photocatalysts,[8,9] the Z-scheme system composed of two or more semiconductors is one of the promising photocatalysts for efficient water splitting, due to advantages of promoting the spatial separation of photogenerated charges and keeping reduction and oxidation reaction at two different reaction sites. In this concept, the water-splitting system could be divided into two components. The photogenerated electrons in the higher conduction band (CB) could be used for $H_2$ evolution, while holes in the lower valence band (VB) for could be used for $O_2$ evolution. Recently, many photocatalytic systems of a Z-scheme have been reported. One kind of Z-scheme system uses a series of interconnected cells for photoelectrochemical water decomposition without electric energy.[10] Another Z-scheme system includes two individual photocatalysts and electron shuttle, for example, $BiVO_4$/Ru-$SrTiO_3$: Rh, Pt-$WO_3$/Pt-$SrTiO_3$: (Cr, Ta), Pt-$SrTiO_3$: Rh/$BiVO_4$, and Pt-$ATaO_2N$(A: Ca, Sr, Ba)[11−14] with the electron shuttle $[Co(bph)_3]^{3+}$/$[Co(bpy)_3]^{2+}$, $IO^{3-}/I^-$, and $Fe^{3+}/Fe^{2+}$; but the competition from redox reaction in solution usually decreases the catalytic activity of those photocatalysts.[15] So it is necessary to construct a hybrid system based on a Z-scheme, which consists of two photocatalysts without redox mediators.

Owing to suitable band gap and CB potential, CdS can be used for $H_2$ production. Because photogenerated electrons could rapidly recombine with holes, the photocatalytic activity, CdS alone is far more exciting. Compared with other photocatalysts, $WO_3$ owns some merits such as its high carrier mobility and chemical stability and thermostability. However, its utilization is limited since it cannot be used for $H_2$ evolution due to lower CB. We note that the $CdS/WO_3$ heterostructure is beneficial to the separation of photogenerated charges.[16] We are also aware that the $CdS/WO_3$ heterostructure has been studied in photocatalytic degradation of dye and photocatalytic $O_2$ evolution.[17] Hence, reports indicate extensive applications of $CdS/WO_3$ for photocatalytic $H_2$ generation from water splitting based on the Z-scheme. Yet, up to now, highly photocatalytic activity of $CdS/WO_3$ for $H_2$ evolution from

Received: June 9, 2014
Revised: August 17, 2014
Published: September 12, 2014

   dx.doi.org/10.1021/cs500794j | ACS Catal. 2014, 4, 3724−3729

water splitting has seldom been reported with lactic acid as electron donor.

In the study, we combined $WO_3$ and CdS to achieve an all-solid-state Z-scheme mechanism. Photocatalytic $H_2$ evolution by using lactic acid as electron donors has been studied under visible light irradiation. The rate of $H_2$ evolution of the optimized CdS/$WO_3$ is 5 times as high as that of CdS. In order to further improve the rate of $H_2$ evolution, Pt was loaded between CdS and $WO_3$. A good $H_2$ evolution rate up to 2900 $\mu$mol $g^{-1}$ $h^{-1}$ was obtained with CdS(20 wt %)/Pt(3 wt %)/$WO_3$. The rate of $H_2$ evolution of the optimized CdS/Pt/$WO_3$ is about 7.9 times the rate of WC20 under visible light irradiation. However, it was surprising to find that the photocatalytic mechanism seems to be different from the one previously reported.[16,17]

## EXPERIMENTAL SECTION

**Catalyst Preparation.** All chemicals are analytical grade reagents and used without further purification.

$WO_3$ nanorods were synthesized by a hydrothermal method. Typically, 1 g of $Na_2WO_4{\cdot}2H_2O$ and 0.2 g of NaCl were added in 30 mL of deionized water and then stirred for 6 h. The pH values of the solution were adjusted to around 2 with concentrated hydrochloric acid and stirred for another 3 h. Then, the solution was transferred into a 50 mL Teflon-lined autoclave. The autoclave was maintained at 180 °C and 24 h. The product was filtered and washed several times with deionized water and absolute ethanol and dried at 50 °C for 10 h.

The Pt/$WO_3$ was prepared by a $NaBH_4$ reduction method.[18] Briefly, $H_2PtCl_6$ aqueous solution (18.71 mmol/L) was a Pt resource. A $NaBH_4$ aqueous was quickly put to the solution to reduce $H_2PtCl_6$ to Pt, and the amount of substance for $NaBH_4$ is ten times as much as that of $H_2PtCl_6$.

The CdS/$WO_3$ or CdS/Pt/$WO_3$ were prepared by an uncomplicated precipitation method. 0.3 g of $WO_3$ or Pt/$WO_3$ was scattered into 30 mL of deionized water. Subsequently, a certain $CdCl_2{\cdot}2.5H_2O$ (cadmium chloride hemipentahydrate) was put in the above solution, and then a certain volume of 42 mM $Na_2S$ aqueous solution was added dropwise. After stirring 1 h, the precipitation was washed and dried. The weight ratios of CdS to $WO_3$ were $R$ = 0, 10, 20, 30, and 100, which are labeled as WC0, WC10, WC20, WC30, and WC100, respectively, and the CdS(20 wt %)/Pt(1 wt %)/$WO_3$, CdS(20 wt %)/Pt(3 wt %)/$WO_3$, and CdS(20 wt %)/Pt(5 wt %)/$WO_3$ are labeled as WPC1, WPC3, and WPC5, respectively. The CdS sample was also synthesized under the same conditions without $WO_3$ (Pt/$WO_3$)

**Characterization.** The field emission scanning electron microscope (FESEM; FEI Company) was applied to measure the morphology of CdS/$WO_3$. The transmission electron microscopy (TEM), high-resolution transmission electron microscopy (HRTEM), and element mappings were conducted with the JEOL JEM-3010 transmission electron microscopy. The crystalline phase was obtained by a X-ray diffractometer (XRD) with a Rigaku D/Max-2550 diffractometer using Cu K$\alpha$ radiation ($\lambda$ = 1.5418 Å). An Escalab 250 spectrometer using monochromatized Al K$\alpha$ excitation was used to character XPS (X-ray photoelectron spectrometer) of CdS/$WO_3$. The UV−vis diffuse reflectance spectrum (UV−vis DRS) of CdS/$WO_3$ (300−800 nm) was detected on a UV−vis−NIR spectrophotometer (Shimadzu UV−3600). The TPV and SPV of CdS/$WO_3$ were carried out on equipment which was reported in our earlier paper.[19,20]

**Photocatalytic Reaction.** The quartz cell was used to test the photocatalytic $H_2$ production. The visible light ($\lambda$ > 400 nm) was provided by 500 W xenon with a UV-cutoff filter. The area of irradiation was 5.3 $cm^2$. The photocatalyst was 0.05 g. The electronic donor was lactic acid. The amount of $H_2$ was obtained on gas chromatography (TOC, $N_2$ as a carrier gas).

## RESULTS AND DISCUSSION

Figure 1 displays a comparison of XRD patterns for the $WO_3$ and CdS/$WO_3$. The hexagonal structure $WO_3$ [JCPDS No. 75-2187] is observed for CdS/$WO_3$. Moreover, with the increase of CdS concentration, the (111), (220), and (300) peaks assigned to CdS of cubic phase are more and more obvious. Besides, peak shifts could not be observed, which indicates that the photocatalyst is made up of CdS and $WO_3$. The diffraction peaks of CdS are tagged with star symbols.

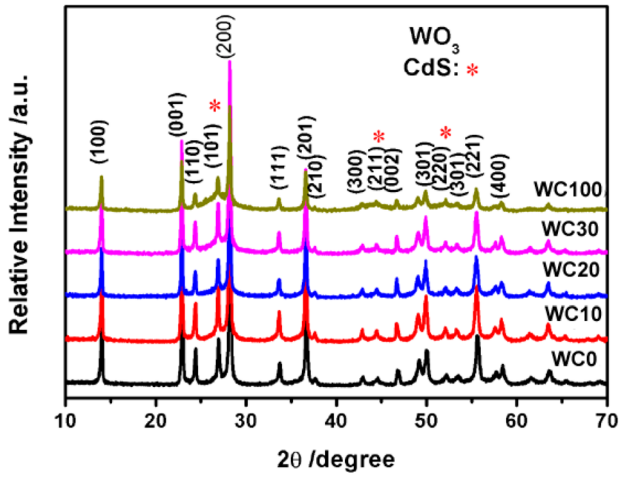


**Figure 1.** XRD patterns of the WC0, WC10, WC20, WC30, and WC100.

The morphology of pure $WO_3$ and CdS(20 wt %)/$WO_3$ was characterized by FESEM. All the samples show nanorods with the lengths of 0.1−3 $\mu$m and diameters of 65−100 nm. Note that the pure $WO_3$ nanorods are smooth (in Figure S1(b)). However, the $WO_3$ nanorods surface is rougher for CdS loaded (in Figure S1(c)). Figure S1(d) shows that many CdS nanoparticles are loaded on the $WO_3$ nanorods. In Figure S1(e), the EDAX of pure $WO_3$ confirms that $WO_3$ is made up of W and O atoms, while the EDAX of CdS(20 wt %)/$WO_3$ exhibits Cd and S besides W and O (Figure S1(f)). Therefore, up to now, the above analyses suggest that CdS is successfully coated on $WO_3$.

To investigate the structural information on CdS/$WO_3$, the TEM images of CdS(20 wt %)/$WO_3$ are conducted (in Figure 2). One can seen in Figure 2(a), the $WO_3$ nanorods closely connect with CdS nanoparticles. The HRTEM of the CdS/$WO_3$ shown in Figure 2(b) heterojunction is formed between CdS and $WO_3$. One can seen in Figure 2(b) (square zone labeled in Figure 2(a)), the lattice fringe of CdS can be identified as 0.336 nm for (111) spacing. What is more, the intimate contact is beneficial to charge transport between CdS and $WO_3$ nanorods.

Figure 3(a) shows the UV−vis DRS of CdS/$WO_3$, $WO_3$, and CdS. The absorption edge of $WO_3$ is at about 460 nm, while


dx.doi.org/10.1021/cs500794j | ACS Catal. 2014, 4, 3724−3729

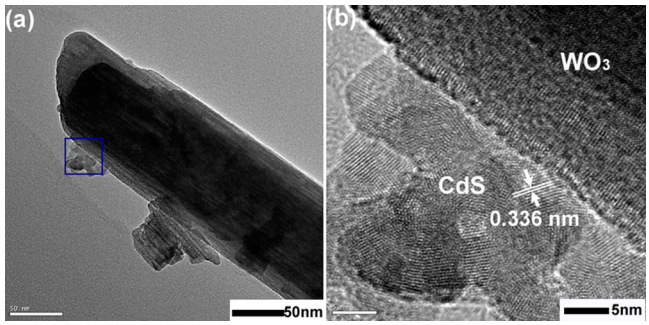


**Figure 2.** TEM images of CdS/$WO_3$ nanorods: (a) TEM image of WC20 and (b) the HRTEM image of CdS nanoparticles and $WO_3$ nanrods.

that of CdS is at about 590 nm. Moreover, an increase of CdS loaded has evident influence on the optical response of CdS/$WO_3$.

The following formula can be used to calculate the bandgap energy for one semiconductor[21]

$$\alpha h\nu = A(h\nu - E_g)^{n/2} \quad (1)$$

where $h\nu$, $\alpha$, $A$, and $E_g$ are light energy, absorption index, constant value, and bandgap energy of semiconductor, respectively. What is more, $n$ relies on the transition type of semiconductor. The $n$ for direct transition is equal to 1, while $n$ is 4 for indirect transition. Therefore, the values of CdS and $WO_3$ are 1 and 4, respectively.[22,23] According to Figure 3(b), $WO_3$ is 2.7 eV, which is consistent with previous work,[24] while $E_g$ of CdS is found to be about 2.1 eV. With increase of CdS, the $E_g$ of CdS/$WO_3$ is closer to that of CdS.

The band structures of CdS and $WO_3$ could be valued with the concepts of electronegativity,[25] and the electronegativity for a semiconductor is defined as the geometrical mean of electronegativity for their constituent atoms. What is more, the electronegativity for one atom could be obtained by calculating the arithmetic mean of the ionization energy and electron affinity.[26] The equations for computing the band structure of a semiconductor are as follows[27,28]

$$E_{CB} = X - E^e - 0.5E_g \quad (2)$$

$$E_{CB} = E_{VB} - E_g \quad (3)$$

where $X$ is the electronegativity for semiconductor, $E_{VB}$ is the VB potential, $E_{CB}$ is the CB potential, and $E^e$ is about 4.5 eV. Computing methods for $X_{CdS}$ and $X_{WO3}$ are shown in the Supporting Information. The $E_{CB}$ and $E_{VB}$ of $WO_3$ are 0.72 and 3.42 V, while the $E_{CB}$ and $E_{VB}$ of CdS are −0.26 and 1.84 V, respectively.

The photocatalytic performances for $H_2$ production of $WO_3$, CdS, and CdS/$WO_3$ are shown in Figure 4. Without light or

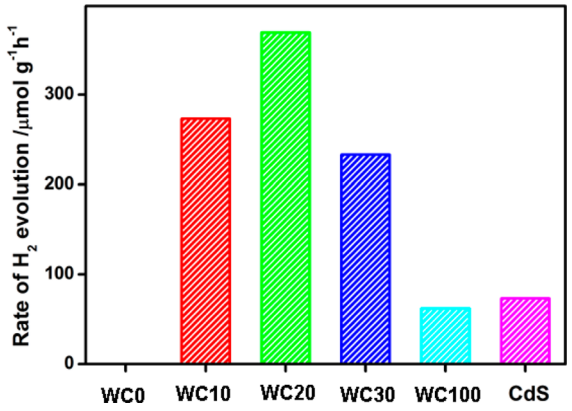


**Figure 4.** Rate of $H_2$ evolution for WC0, WC10, WC20, WC30, WC100, and CdS under irradiation of visible light.

catalyst, no $H_2$ is obtained which implies that $H_2$ generation is a light catalyzed reaction. $WO_3$ alone exhibits no activity for $H_2$ production, due to lower conduction potential. CdS alone displays poor activity (73 $\mu$mol $g^{-1}$ $h^{-1}$) under visible light, due to nanoparticles aggregation and easy recombination photoinduced charges. However, interestingly, the CdS/$WO_3$ composites exhibit higher activity than CdS. Particularly, when the content of CdS is 20 wt %, the WC20 demonstrates the highest rate of 369 $\mu$mol $h^{-1}$ $g^{-1}$, which surpasses that of CdS by more than 5 times. A further increase in the amount for CdS results in a decrease of activity. There are two reasons which may explain this reduction of activity: (I) High content of CdS could hinder $WO_3$ from absorbing light which would undoubtedly weaken the interaction between $WO_3$ and CdS. (II) Overmuch CdS may turn into a recombination center of photoinduced charges, which would cause reduction of activity.[29,30]

As we all know, the noble metals, especially Pt, can promote the $H_2$ evolution efficiency for many photocatalysts. Moreover,

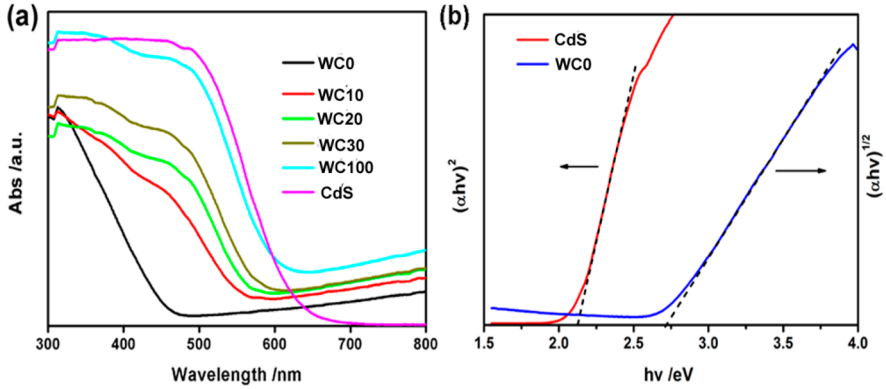


**Figure 3.** (a) UV−visible diffuse reflectance spectra of WC0, WC10, WC20, WC30, WC100, and CdS. (b) Plots of the $(\alpha h\nu)^2$ vs photon energy $(h\nu)$ for CdS, plots of the $(\alpha h\nu)^{1/2}$ vs photon energy $(h\nu)$ for WC0.


dx.doi.org/10.1021/cs500794j | ACS Catal. 2014, 4, 3724−3729

the position of Pt loaded is of importance for the performance of photocatalyst. Rao et al.[31] found that Pt loaded between CdS and ZnO can improve the interfacial charge transfer and CdS/Pt/ZnO shows higher activity than Pt/CdS/ZnO with Pt being loaded on the CdS/ZnO surface. Thus, in order to further improve the activity of $CdS/WO_3$, we first carried out the synthesis of $WO_3$ nanorods. The Pt was subsequently loaded. Finally, the CdS nanoparticles were deposited. The structural information about WPC3 was examined by HRTEM images. Figure 5(a) shows that the $WO_3$ nanorods are loaded with Pt

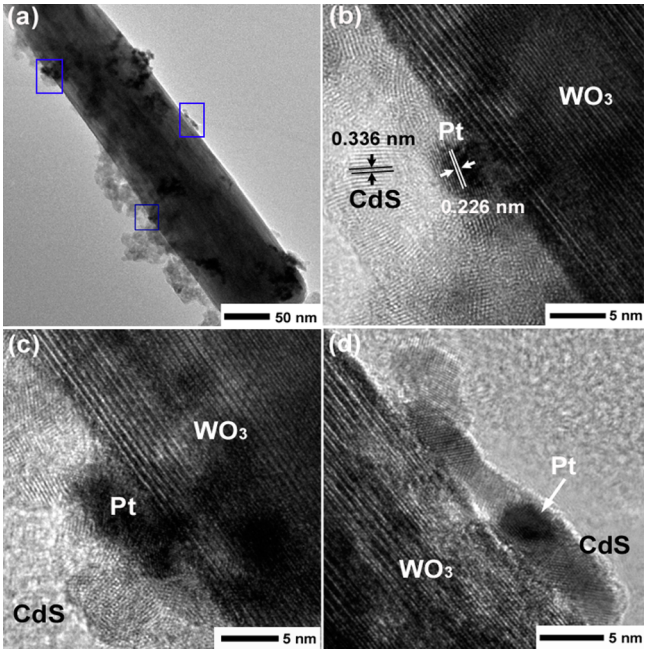


**Figure 5.** (a) TEM image of WPC3 and (b-d) the high resolution TEM image of CdS nanoparticles, Pt nanoparticles, and $WO_3$ nanorods.

and CdS nanoparticles. One can see in Figure 5(b) (square region marked in Figure 5(a)), that the interplanar distance of 0.226 nm is identified as the (111) plane of Pt and Pt is located between CdS and $WO_3$. The EDS mapping of elements was shown in Figure S2. As can be seen, Pt and Cd elements distribute over the whole $WO_3$ surface. Up to now, we have successfully constructed the structure of $CdS/Pt/WO_3$.

So the $H_2$ evolution activity of $CdS/Pt/WO_3$ was further studied with visible light. One can see (in Figure 6), the $H_2$ evolution rate of $CdS/WO_3$ is markedly enhanced by loading Pt, under visible light. When the content of Pt is 3 wt %, the $CdS/Pt/WO_3$ shows the highest $H_2$ generation rate of 2900 $\mu$mol $g^{-1}$ $h^{-1}$, exceeding that of $CdS/WO_3$ by 7.9 times. This may indicate that Pt could play as a bridge between CdS and $WO_3$ for charge transferring which results in enhancement of charge separation efficiency for CdS. The $H_2$ generation activity for WPC3 seems to be higher than previous works, such as $RGO/ZnIn_2S_4$,[32] NiO/CdS,[33] $TiO_2/MoS_2/MG$,[34] and P-$MoS_2$/N-graphene[35] tested under various tested conditions, though fair comparisons should be conducted under the same conditions such as light frequency and optical intensity.

For exploring the synergistic reaction of CdS and $WO_3$ for $H_2$ evolution, we have studied the charge transmit characteristics on the $CdS/WO_3$ surface and at the interface between CdS and $WO_3$ with photovoltaic technology. As shown in

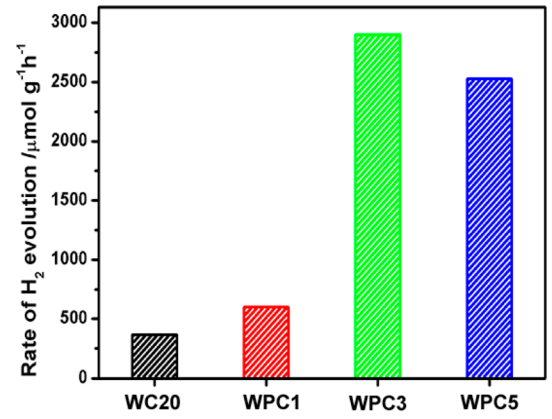


**Figure 6.** Rate of $H_2$ evolution for WC20, WPC1, WPC3, and WPC5 under irradiation of visible light.

Figure 7, the TPV responses for $CdS/WO_3$ and CdS with 355 nm laser illumination are exhibited with a logarithmical time

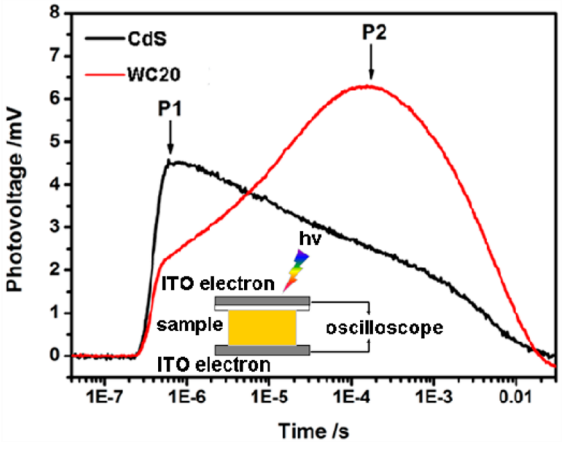


**Figure 7.** TPV of WC20 and CdS. The wavelength and intensity of excitation pluse are 355 nm and 50 $\mu$J, respectively. Inset: schematic setup of TPV measurement.

scale. There are two characteristics for $CdS/WO_3$. (I) Both CdS and $CdS/WO_3$ show positive signals, suggesting characteristics for n-type CdS. (II) Two response peaks (P1 and P2 peaks) can be observed in the TPV responses for WC20. The time value for the P1 peak is shorter than $10^{-6}$ s while that for the P2 peak is longer than $10^{-4}$ s. The photoinduced charges are generated in $CdS/WO_3$ with laser irradiation, and charge separation, which is caused by the electric field of the surface charge zone, produces TPV response ($<10^{-6}$ s).[36] What is more, the TPV response (time > $10^{-4}$ s) corresponds to diffusion voltage.[37] Compared with CdS, the $CdS/WO_3$ shows clear diffusion voltage. When the separating rate of photoinduced charges is the same as the recombination rate, the P2 peak was obtained. The time to the P2 peak is longer; the rate of recombination of photoinduced charges is slower. According to the above analyses, more electrons in $CdS/WO_3$ could take part in the $H_2$ production reaction. Thus, it is reasonable to draw a conclusion that the presence of the interface between $WO_3$ and CdS could effectively depress the photoinduced charge recombination. This is in agreement with the results of our experiments. Figure S4 shows the TPV spectra of WC0 and WPC3. The $WO_3$ shows a weak signal. The time of the P2 peak


dx.doi.org/10.1021/cs500794j | ACS Catal. 2014, 4, 3724−3729

for WPC3 is longer than that of WC20, which means that charge separation efficiency of WPC3 is higher than that of WC20. Therefore, WPC3 shows a higher $H_2$ evolution rate.

Figure 8 shows the SPV spectra of CdS and CdS/$WO_3$. The positive signal suggests that holes transmit to the illumination

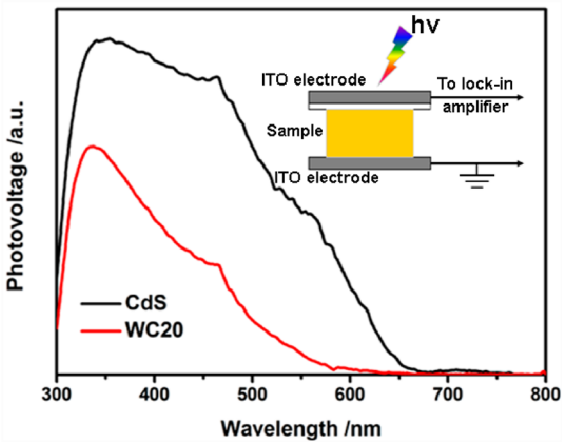


**Figure 8.** SPV of WC20 and CdS.

side of photocatalysts; on the contrary, the negative signal implies that electrons transfer to the surface of the irradiation side for photovoltages. The positive response for CdS (300−590 nm) could be attributed to band gap transition, which is a representative property for CdS (n-type), while the response (590−700 nm) is related to sub-band gap transition (in Figure 8). Compared with CdS, the photoelectric signal of CdS/$WO_3$ shows two properties. On the one hand, the response intensity is reduced, meaning that there are more electrons transferring to the surface. This may indicate that the photogenerated electrons CB for $WO_3$ recombine with the holes of VB for CdS. On the other hand, $K_{CdS/WO3} < K_{CdS}$ ($K$ is the ratio of $I_{456}$ to $I_{365}$ ($I_{456}$ is the photovoltage intensity of a sample at the wavelength of 456 nm)). According to the results, we considered the possible reasons as follows: In general, the penetration depth of light is connected with light energy.[38] The penetration depth for homogeneous light decreases with the increasing light energy. Under the 365 nm light irradiation, compared with the 456 nm light irradiation, the transmission depth is smaller, and the photovoltage response of CdS has more contribution to the photoelectric response of CdS/$WO_3$. While for the 456 nm light irradiation, the penetrating depth is deeper and the interface photovoltage between CdS and $WO_3$ has more contribution to the photoelectric response of CdS/$WO_3$. So the interface makes the reduced photovoltage signal under 456 nm light irradiation. That means that photogenerated electrons have more chances to take part in the photocatalytic $H_2$ evolution which results in increasing the photocatalytic $H_2$ evolution rate of CdS/$WO_3$. This result is an evidence for the interaction between CdS and $WO_3$. However, the detail characteristics are not yet clear and still need further study. As shown in Figure S5, the SPV response of WPC3 is weaker than that of CdS which indicates that more electrons accumulate on the surface of WPC3 compared with CdS. Due to electrons tunnelling and electrons trapped by Pt, the SPV response for WPC3 is stronger than that of WC20, and the $WO_3$ does not show previous photovoltage signals.

According to the previously reported charge transfer mechanism[16,17] between CdS and $WO_3$, the photogenerated electrons will transfer from the conduction of CdS to the conduction of $WO_3$. However, according to previous reports, the work function (WF) for $WO_3$ is higher than the WF of CdS.[39,40] When CdS contacts with $WO_3$, electrons of CdS could transfer to $WO_3$ until their WFs are the same. Then, the interface band bendings are formed (Figure 9a).[36] The CB

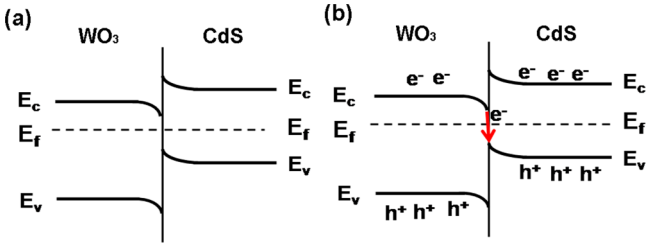


**Figure 9.** (a) The interface band bending diagram between CdS and $WO_3$. (b) The interfacial electron transfer between CdS and $WO_3$.

bending of CdS sets up a potential barrier. Then, when the catalysts are under light irradiation, only the photogenerated electrons in CB of CdS which have the energy to stride over the potential barrier can transport from CdS to $WO_3$. So, the existence of potential barrier goes against the transmission of photogenerated electrons from CB of CdS to CB of $WO_3$. The same principle can be applied to the transfer of photogenerated holes from VB of $WO_3$ to CB of CdS. In contrast, the energy band structure is more beneficial to the transfer of photogenerated electrons from CB of $WO_3$ to VB of CdS (in Figure 9). So, based on the above analyses and results of our experiments, the photocatalytic mechanism of CdS/$WO_3$ for $H_2$ evolution could be as shown in Scheme S1 on the Z-scheme. Under visible light irradiation, the $WO_3$ and CdS are excited and then produce photogenerated electrons and holes, respectively. The photogenerated electrons in $WO_3$ recombine with holes in CdS. As a result, the probability of photogenerated charge recombination can be significantly decreased. More photogenerated electrons in CdS are available to reduce $H^+$ to $H_2$, which results in highly efficient photocatalytic $H_2$ evolution activity.

Our CdS/$WO_3$ is a visible Z-scheme system which is different from CdS/Au/$TiO_2$,[41] because $TiO_2$ cannot be excited by visible light, and our system differs from CdS/Au/$TiO_{0.96}C_{0.04}$.[42] $TiO_{0.96}C_{0.04}$ can be used for $H_2$ evolution, while $WO_3$ cannot be used for $H_2$ evolution. Other closely contacted systems like CdS/ZnO/Pt,[31] CdS/$TiO_2$,[43] CdS/Gr,[44] and CdS/$TaS_2$[45] also exhibit better activity than CdS alone, for enhancing charge separation efficiency in CdS. However, in those systems, photoinduced electrons in CdS transfer from CB of CdS to lower CB, which may decrease reducing capacity of electrons. Our Z-scheme system could not only improve the charge separation efficiency but also make more electrons accumulate in the CB of CdS.

Figure S6 displays the cycle experiments for WC20 and WCP3. Three runs were conducted. Moreover, every 3 h, $N_2$ gas was bubbled in order to purge $H_2$. After three cycles, the $H_2$ generation activity of WC20 and WPC3 has evident reduction which may be caused by photocorrosion of CdS or lactic acid consumption.

## CONCLUSION

In summary, the artificial photosynthesis system which consists of CdS and $WO_3$ is successfully constructed. The CdS/$WO_3$ on


dx.doi.org/10.1021/cs500794j | ACS Catal. 2014, 4, 3724−3729

a Z-scheme mechanism is demonstrated to show high activity for $H_2$ generation with visible radiation. The as-prepared WPC3 photocatalyst in which Pt is introduced to further improve the $H_2$ evolution activity shows a high $H_2$ production rate of 2900 $\mu$mol $g^{-1}$ $h^{-1}$. The construction of a Z-system decreases the probability of charge recombination and increases the lifespan of charges in CdS, thus, leading to the improved $H_2$ generation rate.

## ■ ASSOCIATED CONTENT

### Supporting Information

Figures S1−S6, Table S1, eqs S1−S6, and Scheme S1. This material is available free of charge via the Internet at http://pubs.acs.org.

## ■ AUTHOR INFORMATION


### Corresponding Author

*Phone: +86 431 85168093. E-mail: xietf@jlu.edu.cn.


### Notes

The authors declare no competing financial interest.

## ■ ACKNOWLEDGMENTS

For financial support, we are grateful to the National Natural Science Foundation of China (nos. 21173103 and 51172090) and the National Basic Research Program of China (973 Program) (2013CB632403). This work was also supported by the Science and Technology Developing Funding of Jilin Province (no. 201115012).

## ■ REFERENCES


(1) Esswein, A.; Nocera, D. *Chem. Rev.* **2007**, *107*, 4022−4047.
(2) Chen, X.; Shen, S.; Guo, L.; Mao, S. *Chem. Rev.* **2010**, *110*, 6503−6570.
(3) Kudo, A.; Miseki, Y. *Chem. Soc. Rev.* **2009**, *38*, 253−278.
(4) Meng, F.; Li, J.; Cusing, S.; Zhi, M.; Wu, N. *J. Am. Chem. Soc.* **2013**, *135*, 10286−10289.
(5) Chen, W.; Iyer, S.; Iyer, S.; Sasaki, K.; Wang, C.; Zhu, Y.; Muckerman, J.; Fujita, E. *Energy Environ. Sci.* **2013**, *6*, 1818−1826.
(6) Kong, D.; Cha, J.; Hye, H.; Lee, R.; Cui, Y. *Energy Environ. Sci.* **2013**, *6*, 3553−3558.
(7) Zhang, L.; Xie, T.; Wang, D.; Li, S.; Wang, L.; Chen, L.; Lu, Y. *Int. J. Hydrogen Energy* **2013**, *38*, 11811−11817.
(8) Maeda, K.; Teramura, K.; Lu, D.; Takata, T.; Saito, N.; Inoue, Y.; Domen, K. *Nature* **2006**, *440*, 295.
(9) Kato, H. *J. Am. Chem. Soc.* **2003**, *125*, 3082−3089.
(10) Park, H.; Lee, H.; Leonard, K.; Liu, G.; Bard, A. *ChemPhysChem* **2013**, *14*, 2277−2287.
(11) Sasaki, Y.; Kato, H.; Kudo, A. *J. Am. Chem. Soc.* **2013**, *135*, 5441−5449.
(12) Sayama, K.; Mukasa, K.; Abe, R.; Abe, Y.; Arakawa, H. *J. Photochem. Photobiol., A* **2002**, *148*, 71−77.
(13) Kato, H.; Hori, M.; Konta, K.; Takato, T.; Ohtani, B.; Domen, K. *Chem. Lett.* **2004**, *33*, 1348−1349.
(14) Higashi, M.; Abe, R.; Teramura, K.; Takata, T.; Ohtani, B.; Domen, K. *Chem. Phys. Lett.* **2008**, *452*, 120−123.
(15) Wang, X.; Liu, G.; Chen, Z.; Li, F.; Wang, L.; Lu, G.; Cheng, H. *Chem. Commun.* **2009**, *23*, 3452−3454.
(16) Li, H.; Zhou, Y.; Chen, L.; Luo, W.; Xu, Q.; Wang, X.; Xiao, M.; Zou, Z. *Nanoscale* **2013**, *5*, 11933−11939.
(17) (a) Wang, F.; Wang, Y.; Zhan, X.; Safdar, M.; Gong, J.; He, J. *CrystEngComm* **2014**, *16*, 1389−1394. (b) Kim, H.; Tak, Y.; Senthil, K.; Joo, J.; Jeon, S.; Yong, K. *J. Vac. Sci. Technol. B* **2009**, *27*, 2182−2186.
(18) Zhang, L.; Zheng, R.; Li, S.; Liu, B.; Wang, D.; Wang, L.; Xie, T. *ACS Appl. Mater. Interfaces* **2014**, *6*, 13406−13412.
(19) Li, H.; Wang, D.; Fan, H.; Wang, P.; Jiang, T.; Xie, T. *J. Colloid Interface Sci.* **2011**, *354*, 175−180.
(20) Jiang, T.; Xie, T.; Chen, L.; Fu, Z.; Wang, D. *Nanoscale* **2013**, *5*, 2938−2944.
(21) Butler, M. A. *J. Appl. Phys.* **1977**, *48*, 1914−1920.
(22) González-Borrero, P.; Sato, F.; Medina, A. N.; Baesso, M. L.; Bento, A. C.; Baldissera, G.; Persson, C.; Niklasson, G. A.; Granquist, C. G.; Ferreira da Silva, A. *Appl. Phys. Lett.* **2010**, *96*, 061909.
(23) Ivanov, S.; Piryatinski, A.; Nanda, J.; Tretiak, S.; Zavadil, K.; Wallance, W.; Werder, D.; Kilmov, V. *J. Am. Chem. Soc.* **2007**, *129*, 11708−11719.
(24) Huda, M.; Yan, Y.; Wei, S.; Al-Jassim, M. *Phys. Rev. B* **2009**, *80*, 115118.
(25) Ki, Y. I.; Atherton, S. J.; Brigham, E. S.; Mallouk, T. E. *J. Phys. Chem.* **1993**, *97*, 11802−11810.
(26) Butler, M.; Ginley, D. *J. Electrochem. Soc.* **1978**, *125*, 228.
(27) Lin, X.; Xing, J.; Wang, W.; Shan, Z.; Xu, F.; Huang, F. *J. Phys. Chem. C* **2007**, *111*, 18288−18293.
(28) Tang, J.; Ye, J. *Chem. Phys. Lett.* **2005**, *410*, 104−107.
(29) Zhang, L.; Jiang, T.; Li, S.; Lu, Y.; Wang, L.; Zhang, X.; Wang, D.; Xie, T. *Dalton Trans.* **2013**, *42*, 12998−13003.
(30) Zhang, J.; Yu, J.; Jaroniec, M.; Gong, J. *Nano Lett.* **2012**, *12*, 4584−4589.
(31) Lingampalli, S. R.; Gautam, U.; Rao, C. *Energy Environ. Sci.* **2013**, *6*, 3589−3594.
(32) Ye, L.; Fu, J.; Xu, Z.; Yuan, R.; Li, Z. *ACS Appl. Mater. Interfaces* **2014**, *6*, 3483−3490.
(33) Khan, Z.; Khannam, M.; Vinothkumar, N.; De, M.; Qureshi, M. *J. Mater. Chem.* **2012**, *22*, 12090−12095.
(34) Xiang, Q.; Yu, J.; Jaroniec, M. *J. Am. Chem. Soc.* **2012**, *134*, 6575−6578.
(35) Meng, F.; Li, J.; Cushing, S.; Zhi, M.; Wu, N. *J. Am. Chem. Soc.* **2011**, *135*, 10286.
(36) Kronik, L.; Shapira, Y. *Surf. Sci. Rep.* **1999**, *37*, 1−206.
(37) Timoshenko, V.; Duzhko, V.; Dittrich, T. *Phys. Status Solidi A* **2000**, *182*, 227 2, 227..
(38) Fan, H.; Jiang, T.; Li, H.; Wang, D.; Wang, L.; Zhai, J.; He, D.; Wang, P.; Xie, T. *J. Phys. Chem. C* **2008**, *112*, 6648−6652.
(39) Krőger, M.; Hamwi, S.; Meyer, J.; Riedl, T.; Kowalsky, W.; Kahn, A. *Appl. Phys. Lett.* **2009**, *95*, 123301.
(40) Brillson, L. *Phys. Rev. B* **1978**, *18*, 2431−2446.
(41) Tada, H.; Mitsui, T.; Kiyonaga, T.; Tanska, K. *Nat. Mater.* **2006**, *5*, 782−786.
(42) Yun, H.; Lee, H.; Kim, N.; Lee, D.; Yu, S.; Yi, J. *ACS Nano* **2011**, *5*, 4084−4090.
(43) Jang, J.; Li, W.; Oh, S.; Lee, J. *Chem. Phys. Lett.* **2006**, *425*, 278−282.
(44) Li, Q.; Guo, B.; Yu, J.; Ran, J.; Zhang, B.; Yan, H.; Gong, J. *J. Am. Chem. Soc.* **2011**, *133*, 10878−10884.
(45) Gupta, U.; Rao, B.; Maitra, U.; Prasad, B.; Rao, C. *Chem. Asian J.* **2014**, *9*, 1311−1315.